Inorg. Chem. **2004**, *43*, 7315–7323

A Family of Mn_{16} Single-Molecule Magnets from a Reductive Aggregation Route

Philippa King,[†] Wolfgang Wernsdorfer,[‡] Khalil A. Abboud,[†] and George Christou*[,†]

Department of Chemistry, University of Florida, Gainesville, Florida 32611-7200, and Laboratoire Louis Néel-CNRS, BP 166, 25 Avenue des Martyrs, 38042 Grenoble, Cedex 9, France

Received August 9, 2004

The synthesis and magnetic properties of three isostructural hexadecametallic manganese clusters $[Mn_{16}O_{16}(OMe)_6(O_2CCH_2Ph)_{16}(MeOH)_6]$ (**1**), $[Mn_{16}O_{16}(OMe)_6(O_2CCH_2Cl)_{16}(MeOH)_6]$ (**2**), and $[Mn_{16}O_{16}(OMe)_6(O_2CCH_2Br)_{16}(MeOH)_6]$ (**3**) are reported. The complexes were prepared by a reductive aggregation reaction involving phenylacetic acid, chloroacetic acid or bromoacetic acid, and $NBu^n_4MnO_4$ in MeOH. Complex **1** crystallizes in the monoclinic space group *C*2/*c* and consists of 6 Mn^{IV} and 10 Mn^{III} ions held together by 14 μ_3-O^{2-}, 2 μ-O^{2-}, 4 μ-MeO^-, and 2 μ-$O_2CCH_2Ph^-$ groups. The remaining 14 μ-$O_2CCH_2Ph^-$ ligands, 2 μ-MeO^- groups, and 6 terminal MeOH molecules constitute the peripheral ligation in the complex. Variable-temperature, solid-state dc magnetic susceptibility measurements on **1**–**3** in the temperature range 5.0–300 K reveal that all three complexes are dominated by intramolecular antiferromagnetic exchange interactions. Low-lying excited states preclude an exact determination of the spin ground state for **1**–**3** by magnetization measurements. Alternating current susceptibility measurements at zero dc field in the temperature range 1.8–10 K and a 3.5 G ac field oscillating at frequencies in the 5–1488 Hz range display, at temperatures below 3 K, a nonzero, frequency-dependent χ_M'' signal for complexes **1**–**3**, with the peak maxima lying at temperatures less than 1.8 K. Single-crystal magnetization versus dc field scans down to 0.04 K for complex **1** show hysteresis behavior at <1 K, establishing **1** as a new member of the SMM family. No clear steps characteristic of quantum tunneling of magnetization (QTM) were observed in the hysteresis loops.

Introduction

The synthesis of paramagnetic Mn carboxylate clusters has become the focus of much attention since the discovery that some molecules can behave as nanoscale magnets.[1] In order to do so, a molecule must display slow magnetization relaxation (below its blocking temperature). This behavior results from a large ground spin state (*S*) combined with a large and negative Ising (or easy-axis) type of magnetoanisotropy, as measured by the axial zero-field splitting parameter *D*. This combination leads to a significant barrier (*U*) to magnetization reversal, its maximum value given by $S^2|D|$ or $(S^2 - {}^1/_4)|D|$ for integer and half-integer spin, respectively.[2] In practice, the actual or effective barrier U_{eff} is less than *U* because of quantum tunneling of the magnetization (QTM) through the barrier via higher lying M_S levels of the spin *S* manifold. Experimentally, a single-molecule magnet (SMM) shows superparamagnet-like properties, exhibiting both a frequency-dependent out-of-phase ac magnetic susceptibility signal and hysteresis in a plot of magnetization versus applied dc magnetic field. Although complexes displaying SMM behavior are known with a number of metals,[3] homometallic manganese carboxylate clusters have to date proven to be the most fruitful source of SMMs. Examples include the archetypal $[Mn_{12}O_{12}(O_2CR)_{16}(H_2O)_4]$ (R = various) family,[1,2,4] Mn_2,[5] Mn_4,[6] Mn_6,[7] Mn_9,[8] Mn_{16},[9] Mn_{22},[10] Mn_{25},[11] Mn_{30},[12] and Mn_{84}[13] clusters.

As part of our continuing research into new preparative routes to high nuclearity species with potentially interesting structural and/or magnetic properties, we have recently turned our attention to a novel synthetic approach in which a high

* To whom correspondence should be addressed. E-mail: christou@chem.ufl.edu.
† University of Florida.
‡ Laboratoire Louis Néel-CNRS.

(1) Christou, G.; Gatteschi, D.; Hendrickson, D. N.; Sessoli, R. *MRS Bull.* **2000**, *25*, 66.

(2) (a) Sessoli, R.; Gatteschi, D.; Caneschi, A.; Novak, M. A. *Nature* **1993**, *365*, 141. (b) Sessoli, R.; Ysai, H.-L.; Schake, A. R.; Wang, S.; Vincent, J. B.; Folting, K.; Gatteschi, D.; Christou, G.; Hendrickson, D. N. *J. Am. Chem. Soc.* **1993**, *115*, 1804.

10.1021/ic048906j CCC: $27.50
Published on Web 10/20/2004

oxidation state Mn source ($NBu^n_4MnO_4$) is reduced by MeOH in the presence of excess carboxylic acid. It was believed, and subsequently proven, that this technique had the potential to lead to the isolation of high oxidation state Mn clusters as the MnO_4^- was progressively reduced and aggregation occurred. Indeed, the initial success of this reductive aggregation approach in providing a new type of Mn_{12} cluster has recently been reported.[14] In the present work, we show that this procedure also provides a convenient route to Mn_{16} complexes of general formula $[Mn_{16}O_{16}(OMe)_6(O_2CR)_{16}(MeOH)_6]$ (R = CH_2Ph (**1**), CH_2Cl (**2**), CH_2Br (**3**)). In the past, such compounds,[1,7,15] including the isostructural R = Me Mn_{16} cluster previously reported by Murray et al.,[9] were synthesized by the reaction of Mn^{II} with $KMnO_4$ or $NBu^n_4MnO_4$ in the presence of appropriate ligands. This is a comproportionation reaction involving Mn^{II} ions being oxidized while the Mn^{VII} ions are reduced, resulting in a product that contains Mn^{III} and/or Mn^{IV} centers. In contrast, the present procedure represents a single-source route to polynuclear Mn clusters. We herein describe the preparation, structure, and detailed magnetic properties of Mn_{16} complexes **1**−**3**, which are new additions to the family of SMMs.

Experimental Section

Syntheses. All manipulations were performed under aerobic conditions using chemicals as received, unless otherwise stated. $NBu^n_4MnO_4$ was prepared as previously reported.[16]

$[Mn_{16}O_{16}(OMe)_6(O_2CCH_2Ph)_{16}(MeOH)_6]$ (1). To a stirred solution of phenylacetic acid (2.79 g, 20.5 mmol) in MeOH (7.5 mL) was added solid $NBu^n_4MnO_4$ (0.50 g, 1.4 mmol) in small portions, resulting in a dark purple solution that quickly turned dark brown. After being stirred for 5 min, the solution was left undisturbed at ambient temperature for 2 days, during which time large black crystals of $[Mn_{16}O_{16}(OMe)_6(O_2CCH_2Ph)_{16}(MeOH)_6]\cdot 5MeOH$ grew. Yield 24.4 mg, 7.5%. The crystals of **1**·5MeOH were maintained in the mother liquor for X-ray crystallography and other single-crystal studies, or collected by filtration, washed with EtOH (MeOH causes precipitation), and dried in vacuo. Vacuum-dried material is hygroscopic and analyzed as **1**·$4H_2O$. Anal. Calcd (Found) for **1**·$4H_2O$: C, 44.86 (44.82); H, 4.22 (3.91)%. Selected IR data (KBr, cm^{-1}): 3426(w), 3061(s), 3026(s), 1575(m), 1533(m), 1496(s), 1454(s), 1413(s), 1394(s), 1293(m), 1188(w), 1122(s), 1075(s), 1030(s), 843(s), 706(s), 598(s), 524(m).

$[Mn_{16}O_{16}(MeO)_6(O_2CCH_2Cl)_{16}(MeOH)_6]$ (2). The procedure was the same as that employed for complex **1**, except that chloroacetic acid (1.94 g, 20.5 mmol) was employed. Black crystals were again obtained. The crystals were maintained in the mother liquor for X-ray crystallography and other single-crystal studies, or collected by filtration, washed with EtOH, and dried in vacuo. Yield 31 mg, 12%. Anal. Calcd (Found) for **2**: C, 17.56 (17.51); H, 2.48 (2.38)%. Selected IR data (KBr, cm^{-1}): 3420 (w), 2956 (m), 1733 (m), 1599 (m), 1558 (s), 1431 (s), 1397 (s), 1260 (s), 1015 (m), 933 (m), 794 (s), 693 (s), 596 (s).

$[Mn_{16}O_{16}(MeO)_6(O_2CCH_2Br)_{16}(MeOH)_6]\cdot 8H_2O$ (3·$8H_2O$). The procedure was the same as that employed for complex **1**, except that bromoacetic acid (2.85 g, 20.5 mmol) was employed. Dark brown needles were obtained. The crystals were maintained in the mother liquor for X-ray crystallography and other single-crystal

(3) (a) Powell, A. K.; Heath, S. L.; Gatteschi, D.; Pardi, L.; Sessoli, R.; Spina, G.; Del Giallo, F.; Pieralli, F. *J. Am. Chem. Soc.* **1995**, *117*, 2491. (b) Gatteschi, D.; Sessoli, R.; Cornia, A. *Chem. Commun.* **2000**, 725. (c) Oshio, H.; Hoshino, N.; Ito, T. *J. Am. Chem. Soc.* **2000**, *122*, 12602. (d) Cadiou, C.; Murrie, M.; Paulsen, C.; Villar, V.; Wernsdorfer, W.; Winpenny, R. E. P. *Chem. Commun.* **2001**, 2666. (e) Ochsenbein, S. T.; Murrie, M.; Rusanov, E.; Stoeckli-Evans, H.; Sekine, C.; Güdel, H. U. *Inorg. Chem.* **2002**, *41*, 4604. (f) Sokol, J. J.; Hee, A. G.; Long, J. R. *J. Am. Chem. Soc.* **2002**, *124*, 7656. (g) Boudalis, A. K.; Donnadieu, B.; Nastopoulos, V.; Clemente-Juan, J. M.; Mari, A.; Sanakis, Y.; Tuchagues, J. P.; Perlepes, S. P. *Angew. Chem., Int. Ed.* **2004**, *43*, 2266. (h) Osa, S.; Kido, T.; Matsumoto, N.; Re, N.; Pochaba, A.; Mrozinski, J. *J. Am. Chem. Soc.* **2004**, *126*, 420. (i) Berlinguette, C. P.; Vaughn, D.; Canada-Vilalta, C.; Galan-Mascaras, J. R.; Dunbar, K. R. *Angew. Chem., Int. Ed.* **2003**, *42*, 1523. (j) Andres, H.; Basler, R.; Blake, A. J.; Cadiou, C.; Chaboussant, G.; Grant, C. M.; Gudel, H.-U.; Murrie, M.; Parsons, S.; Paulsen, C.; Semadini, F.; Villar, V.; Wernsdorfer, W.; Winpenny, R. E. P. *Chem. Eur. J.* **2002**, *8*, 4867. (k) Dendrinou-Samara, C.; Alexiou, M.; Zaleski, C. M.; Kampf, J. W.; Kirk, M. L.; Kessissoglou, D. P.; Pecoraro, V. L. *Angew. Chem., Int. Ed.* **2003**, *42*, 3763.

(4) (a) Eppley, H. J.; Tsai, H.-L.; de Vries, N.; Folting, K.; Christou, G.; Hendrickson, D. N. *J. Am. Chem. Soc.* **1995**, *117*, 301. (b) Aubin, S. M. J.; Spagna, S.; Eppley, H. J.; Sager, R. E.; Christou, G.; Hendrickson, D. N. *Chem. Commun.* **1998**, 803. (c) Aubin, S. M. J.; Sun, Z.; Pardi, L.; Krzystek, J.; Folting, K.; Brunel, L.-C.; Rheingold, A. L.; Christou, G.; Hendrickson, D. N. *Inorg. Chem.* **1999**, *38*, 5329. (d) Soler, M.; Chandra, S. K.; Ruiz, D.; Davidson, E. R.; Hendrickson, D. N.; Christou, G. *Chem. Commun.* **2000**, 2417. (e) Boskovic, C.; Pink, M.; Huffman, J. C.; Hendrickson, D. N.; Christou, G. *J. Am. Chem. Soc.* **2001**, *123*, 9914. (f) Artus, P.; Boskovic, C.; Yoo, J.; Streib, W. E.; Brunel, L.-C.; Hendrickson, D. N.; Christou, G. *Inorg. Chem.* **2001**, *40*, 4199. (g) Soler, M.; Wernsdorfer, W.; Abboud, K. A.; Huffman, J. C.; Davidson, E. R.; Hendrickson, D. N.; Christou, G. *J. Am. Chem. Soc.* **2003**, *125*, 3576. (h) Chakov, N. E.; Abboud, K. A.; Zakharov, L. N.; Rheingold, A. L.; Hendrickson, D. N.; Christou, G. *Polyhedron* **2003**, *22*, 1759. (i) Brockman, J. T.; Abboud, K. A.; Hendrickson, D. N.; Christou, G. *Polyhedron* **2003**, *22*, 1765. (j) Soler, M.; Wernsdorfer, W.; Abboud, K. A.; Hendrickson, D. N.; Christou, G. *Polyhedron* **2003**, *22*, 1777. (k) Morello, A.; Bakharev, O. N.; Brom, H. B.; de Jongh, L. J. *Polyhedron* **2003**, *22*, 1745.

(5) Miyasaka, H.; Clérac, R.; Wernsdorfer, W.; Lecren, L.; Bonhomme, C.; Sugiura, K.; Yamashita, M. A. *Angew. Chem., Int. Ed.* **2004**, *43*, 2801.

(6) (a) Aubin, S. M. J.; Wemple, M. W.; Adams, D. M.; Tsai, H.-L.; Christou, G.; Hendrickson, D. N. *J. Am. Chem. Soc.* **1996**, *118*, 7746. (b) Aubin, S. M.; Gilley, N. R.; Pardi, L.; Krzystek, J.; Wemple, M. W.; Brunel, L. C.; Marple, M. B.; Christou, G.; Hendrickson, D. N. *J. Am. Chem. Soc.* **1998**, *120*, 4991. (c) Brechin, E. K.; Yoo, J.; Huffman, J. C.; Hendrickson, D. N.; Christou, G. *Chem Commun.* **1999**, 783. (d) Yoo, J.; Brechin, E. K.; Yamaguchi, A.; Nakano, M.; Huffman, J. C.; Maniero, A. L.; Brunel, L.-C.; Awaga, K.; Ishimoto, H.; Christou, G.; Hendrickson, D. N. *Inorg. Chem.* **2000**, *39*, 3615. (e) Yoo, J.; Yamaguchi, A.; Nakano, M.; Krzystek, J.; Streib, W. E.; Brunel, L.-C.; Ishimoto, H.; Christou G.; Hendrickson, D. N. *Inorg. Chem.* **2001**, *40*, 4604. (f) Yang, E.; Harden, N.; Wernsdorfer, W.; Zakharov, L.; Brechin, E. K.; Rheingold, A. L.; Christou, G.; Hendrickson, D. N. *Polyhedron* **2003**, *22*, 1857. (g) Wittick, L. M.; Murray, K. S.; Moubaraki, B.; Batten, S. R.; Spiccia, L.; Berry, K. J. *J. Chem. Soc., Dalton Trans.* **2004**, *7*, 1003.

(7) Milios, C. J.; Raptopoulou, C. P.; Terzis, A.; Lloret, F.; Vicente, R.; Perlepes, S. P.; Escuer, A. *Angew. Chem., Int. Ed.* **2003**, *43*, 210.

(8) Brechin, E. K.; Soler, S.; Davidson, J.; Hendrickson, D. N.; Parsons, S.; Christou, G. *Chem. Commun.* **2002**, 2252.

(9) Price, D. J.; Batten, S. R.; Moubaraki, B.; Murray, K. S. *Chem. Commun.* **2002**, 762.

(10) Murugesu, M.; Raftery, J.; Wernsdorfer, W.; Christou, G.; Brechin, E. K. *Inorg. Chem.* **2004**, *43*, 4203.

(11) Murugesu, M.; Habrych, M.; Wernsdorfer, W.; Abboud, K. A.; Christou, G. *J. Am. Chem. Soc.* **2004**, *126*, 4766.

(12) Soler, M.; Rumberger, E.; Folting, K.; Hendrickson, D. N.; Christou, G. *Polyhedron* **2001**, *20*, 1365.

(13) Tasiopoulos, A. J.; Vinslava, A.; Wernsdorfer, W.; Abboud, K. A.; Christou, G. *Angew. Chem., Int. Ed.* **2004**, *43*, 2117.

(14) Tasiopoulos, A. J.; Wernsdorfer, W.; Abboud, K. A.; Christou, G. *Angew. Chem., Int. Ed.*, in press.

(15) Mukhopadhyay, S.; Gandhi, B. A.; Kirk, M. L.; Armstrong, W. H. *Inorg. Chem.* **2003**, *42*, 8171.

(16) (a) Sala, T.; Sargent, M. V. *Chem. Commun.* **1978**, 253. (b) Vincent, J. B.; Chang, H. R.; Folting, K.; Huffman, J. C.; Christou, G.; Hendrickson, D. N. *J. Am. Chem. Soc.* **1987**, *109*, 5703.

Table 1. Crystallographic Data for Complex **1**

formula[a]	$C_{145.25}H_{174.25}Mn_{16}O_{65}$	V, Å^3	16237.8(16)
fw, g/mol[a]	3839.14	Z	4
space group	$C2/c$	T, K	173(2)
a, Å	35.2566(18)	radiation, Å [b]	0.71073
b, Å	20.1227(11)	ρ_{calc}, g/cm^3	1.570
c, Å	27.8640(16)	μ, mm^{-1}	1.286
α, deg	90.00	R_1[c,d]	0.0509
β, deg	116.130(2)	wR_2[e]	0.1445
γ, deg	90.00		

[a] Including solvate molecules. [b] Graphite monochromator. [c] $I > 2\sigma(I)$. [d] $R1 = 100\sum(||F_o| - |F_c||)/\sum|F_o|$. [e] $wR_2 = 100[\sum[w(F_o^2 - F_c^2)^2]/\sum[w(F_o^2)^2]]^{1/2}$, $w = 1/[\sigma^2(F_o^2) + (ap)^2 + bp]$, where $p = [\max(F_o^2, 0) + 2F_c^2]/3$.

studies, or collected by filtration, washed with EtOH, and dried in vacuo. Yield 20 mg, 6%. Anal. Calcd (Found) for **3**·8H_2O: C, 13.67 (13.33); H, 2.34 (1.90)%. Selected IR data (KBr, cm^{-1}): 3446 (w), 2952 (m), 1738 (m), 1594 (m), 1558 (s), 1419 (m), 1218 (s), 1121 (m), 1014 (m), 895 (s), 686 (s), 597 (m).

X-ray Crystallography. Data were collected on a Siemens SMART PLATFORM equipped with a CCD area detector and a graphite monochromator utilizing Mo Kα radiation ($\lambda = 0.71073$ Å). Suitable crystals of **1**·5MeOH were attached to glass fibers using silicone grease and transferred to a goniostat where they were cooled to 173 K for data collection. An initial search of reciprocal space revealed a monoclinic cell; the choice of space group $C2/c$ was confirmed by the subsequent solution and refinement of the structure. Cell parameters were refined using up to 8192 reflections. A full sphere of data (1850 frames) was collected using the ω-scan method (0.3° frame width). The first 50 frames were remeasured at the end of data collection to monitor instrument and crystal stability (maximum correction on I was <1%). Absorption corrections by integration were applied on the basis of measured indexed crystal faces.

The structure was solved by direct methods in *SHELXTL6*,[17] and refined using full-matrix least squares. The non-H atoms were treated anisotropically, whereas the hydrogen atoms were placed in calculated, ideal positions and refined as riding on their respective carbon atoms. The asymmetric unit consists of half a Mn_{16} cluster and 2.5 MeOH molecules. One MeOH is disordered about a 2-fold rotation axis, and the other two are disordered over two sites each but their O atoms could not be distinguished from the methyl C atoms. Thus, they were both refined as C atoms. The six central Mn ions are Mn^{IV} while the rest of the Mn centers are Mn^{III}; there are 16 ligands, 14 O^{2-} groups, two MeO^- groups bridging Mn1 and Mn7 (and their symmetry equivalents), a MeO^- group on O10 (and its symmetry equivalent), and a MeO^- and O^{2-} group disordered over the O19 and O22 positions (and their symmetry equivalents). There are also six terminal MeOH ligands, one of which is disordered about two sites whose occupancies were refined and then fixed in the final refinement model at a 70/30 ratio. A total of 955 parameters were included in the refinement on F^2 using 11921 reflections with $I > 2\sigma(I)$ to yield R_1 and wR_2 of 5.09% and 14.45%, respectively. Unit cell data and details of the structure refinements for **1** are listed in Table 1.

Other Studies. Infrared spectra were recorded in the solid state (KBr pellets) on a Nicolet Nexus 670 FTIR spectrometer in the 400−4000 cm^{-1} range. Elemental analyses (C, H, and N) were performed by the in-house facilities of the University of Florida Chemistry Department. Variable-temperature dc and ac magnetic susceptibility data were collected at the University of Florida using a Quantum Design MPMS-XL SQUID susceptometer equipped with a 7 T magnet and operating in the 1.8−300 K range. Samples were embedded in solid eicosane to prevent torquing. Magnetization versus field and temperature data were fit using the program MAGNET.[18] Pascal's constants were used to estimate the diamagnetic correction, which was subtracted from the experimental susceptibility to give the molar paramagnetic susceptibility (χ_M). Studies at ultralow temperatures (<1.8 K) were performed on single crystals at Grenoble using an array of micro-SQUIDs.[19] The high sensitivity of this magnetometer allows the study of single crystals of SMMs of the order of 10−500 μm; the field can be applied in any direction by separately driving three orthogonal coils.

Results and Discussion

Syntheses. A commonly used synthetic procedure for the preparation of high oxidation state manganese clusters, such as Mn_6,[7,15] Mn_{12},[1] and Mn_{16},[9] is the comproportionation reaction of a Mn^{II} source with MnO_4^- in the presence of appropriate ligand groups. This is a convenient, general procedure involving oxidation of Mn^{II} ions and concomitant reduction of Mn^{VII} ions, producing a product at the Mn^{III} and/or Mn^{IV} oxidation level. The Mn^{II}/Mn^{VII} reaction ratio can readily be varied, and mixed-valent Mn^{IV}/Mn^{III} [20] and Mn^{III}/Mn^{II} [6e,f] complexes can also be obtained. As part of our general search of new synthetic procedures to Mn_x clusters, the present procedure was developed in which the Mn^{II} source was omitted and MeOH was used as both the reducing agent for Mn^{VII} and as a potential source of MeO^- bridging ligands, in the presence also of excess carboxylic acid to prevent formation of manganese oxides and/or hydroxides. The procedure proved its worth with the synthesis of $(NBu^n_4)_2[Mn_{12}O_{12}(OMe)_2(O_2CPh)_{16}(H_2O)_2]$ when benzoic acid was employed;[14] this is a new cluster type and SMM not available, at least to date, by any other route. With an initial success at hand providing proof-of-feasibility, this new reductive aggregation procedure was subjected to further investigation by the use of other carboxylic acids. It was subsequently found that the reaction of phenylacetic acid, chloroacetic acid, and bromoacetic acid with $NBu^n_4MnO_4$ in MeOH gave dark brown solutions from which the corresponding $[Mn_{16}O_{16}(OMe)_6(O_2CR)_{16}(MeOH)_6]$ complexes **1**−**3** were obtained. The yields were low (6−12%), but the reactions are reproducible and have the advantage that the products crystallize as well-formed crystals directly from the reaction solutions without the need to add a second solvent. We were thus happy to sacrifice yield in exchange for pure crystals.

The reactions are clearly very complicated, and the reaction solution likely contains a complicated mixture of several species in equilibrium, with factors such as relative solubility, lattice energies, crystallization kinetics, and others determining the identity of the isolated product. One (or more) of these factors is undoubtedly the reason that changing the carboxylic acid used from benzoic acid to the ones employed in the present work causes a major change in the isolated

(17) (a) Sheldrick, G. M. *SHELXL-97*; University of Göttingen: Germany, 1997. (b) Spek, A. L. *Acta Crystallogr., Sect. A.* **1990**, *46*, C34.

(18) Davidson, E. R. *MAGNET*; Indiana University.

(19) Wernsdorfer, W. *Adv. Chem. Phys.* **2001**, *118*, 99.

(20) Bolcar, M. A.; Aubin, S. M. J.; Folting, K.; Hendrickson, D. N.; Christou, G. *Chem. Commun.* **1997**, 1485.

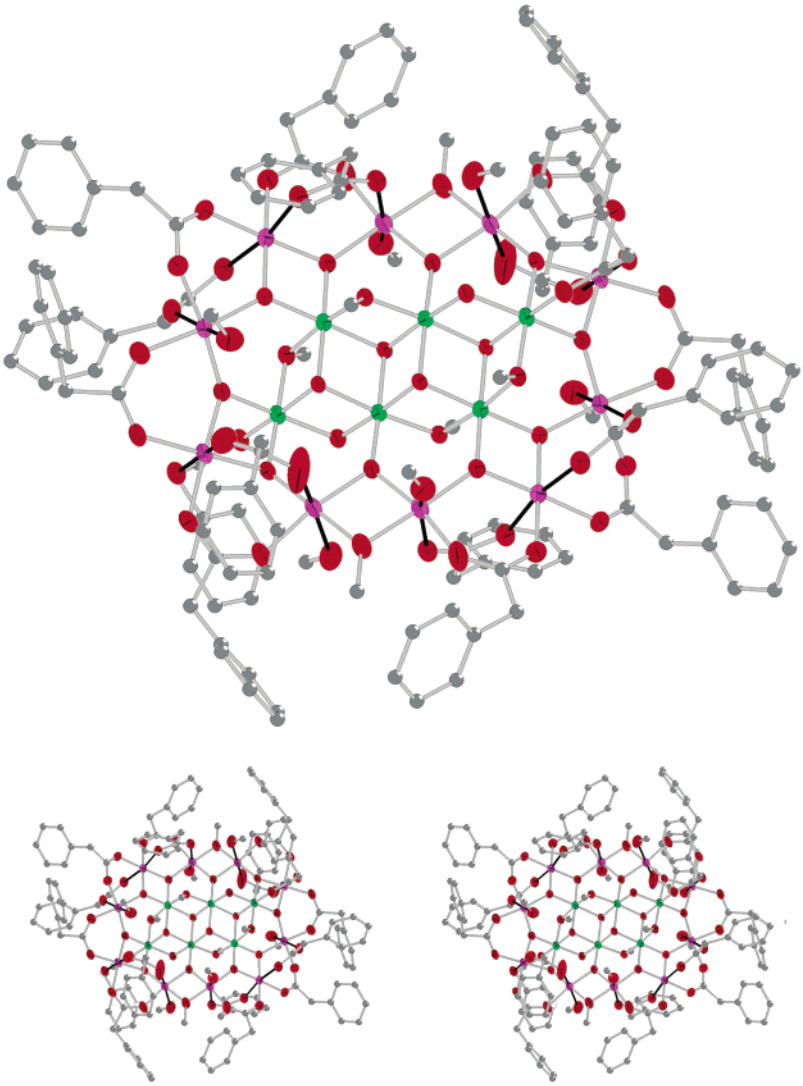

Figure 1. ORTEP representation and stereopair of **1** at the 50% probability level. Hydrogen atoms have been omitted for clarity. Color code: Mn^{IV} green; Mn^{III} purple; O red; C gray.

product from a Mn_{12} species to a Mn_{16} one. The overall formation of complexes **1**−**3** is summarized in eq 1. Presumably, the MeOH is oxidized to formaldehyde and/or formic acid

$$16MnO_4^- + 16RCO_2H + 12MeOH + 74H^+ + 58e^- \rightarrow [Mn_{16}O_{16}(OMe)_6(O_2CR)_{16}(MeOH)_6] + 48H_2O \quad (1)$$

but we have not sought to identify these in the reaction filtrates. A crucial point for the successful attainment of this series of Mn_{16} clusters is the use of very small quantities of MeOH; when more dilute solutions were employed, brown precipitates of manganese oxides/hydroxides were obtained. The latter were also obtained when EtOH was used in place of MeOH in otherwise identical reactions. 2-Propanol led to bleaching of the reaction solutions; i.e., the MnO_4^- was reduced all the way to Mn^{II}.

The three carboxylic acids that were employed, phenylacetic acid ($pK_a = 4.28$), chloroacetic acid ($pK_a = 2.85$), and bromoacetic acid ($pK_a = 2.69$), are all derivatives of acetic acid ($pK_a = 4.76$), and it is thus interesting that when acetic acid itself was used, the product was the previously reported cluster $[Mn_{84}O_{72}(O_2CMe)_{78}(OMe)_{24}(MeOH)_{12}(H_2O)_{42}(OH)_6]$.[13] This contrasts with the fact that it was the acetate cluster $[Mn_{16}O_{16}(OMe)_6(O_2CMe)_{16}(MeOH)_3(H_2O)_3]$ that was obtained by Murray and co-workers[9] from the comproportionation reaction of $Mn(NO_3)_2$ and $NBu^n_4MnO_4$ in excess MeOH; Murray's compound is essentially isostructural with **1**−**3**, except for the terminal H_2O molecules replacing three of the MeOH molecules. Finally, either a significant increase or decrease in the acid-to-MnO_4^- ratio employed in the synthesis of **1**−**3** leads to production of manganese oxide/hydroxide precipitates and essentially colorless mother liquor. However, **1**−**3** are still obtained when the $NBu^n_4MnO_4$ is replaced by $KMnO_4$.

Description of the Structure. An ORTEP representation of the complete Mn_{16} molecule of **1** and a stereopair are provided in Figure 1. A labeled ORTEP of the core and a side view are provided in Figure 2. Selected interatomic distances and angles are listed in Table 2.

Complex **1**·5MeOH crystallizes in the monoclinic space group *C*2/*c* with the Mn_{16} cluster lying on an inversion center.

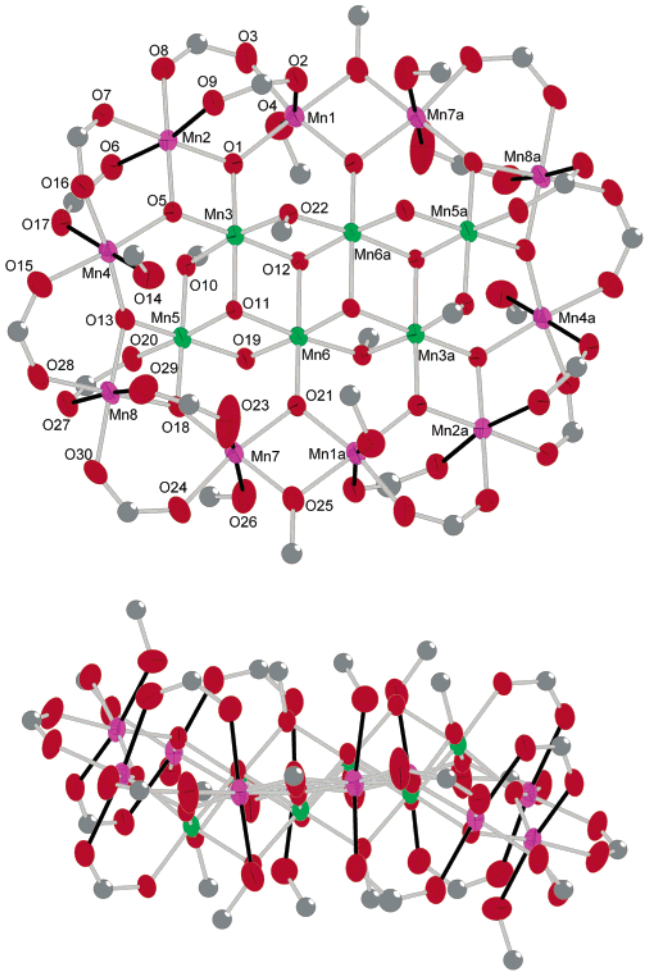

Figure 2. (Top) Labeled ORTEP representation of the core of **1** at the 50% probability level. (Bottom) Side view of the core of **1** showing its chairlike nature and the parallel alignment of the Mn^{III} Jahn−Teller elongation axes (solid black bonds) perpendicular to the plane. Color code: Mn^{IV} green; Mn^{III} purple; O red; C gray.

There is a roughly planar core comprising 6 Mn^{IV} and 10 Mn^{III} ions bridged by 14 μ_3-O^{2-}, 2 μ-O^{2-}, 6 μ-MeO^-, and 16 μ-$PhCH_2CO_2^-$ groups. The six Mn^{IV} ions, Mn3, Mn5, Mn6, and their symmetry equivalents, are located within a central $[Mn^{IV}_6(\mu_3\text{-}O)_4(\mu\text{-}O)_2(\mu\text{-}MeO)_4]^{8+}$ core, with the six Mn^{IV} ions planar and the bridging O atoms above and below this plane. There is disorder in the core, involving a MeO^- and an O^{2-} group being disordered equally over the two positions O19 and O22. The structure of this central $[Mn^{IV}_6(\mu_3\text{-}O)_4(\mu\text{-}O)_2(\mu\text{-}MeO)_4]^{8+}$ core is reminiscent of the planar CdI_2-type sheet structure, as indeed is known for Mn^{IV} in the mineral lithiophorite $(Al,Li)MnO_2(OH)_2$.[21] The structure of the related mineral chalcophanite, $ZnMn_3O_7\cdot 3H_2O$, is similar, but one in every seven Mn^{IV} sites is vacant.[22]

Encapsulating the central core is a nonplanar ring of 10 Mn^{III} atoms (Mn1, Mn2, Mn4, Mn7, Mn8, and their symmetry equivalents) to which it is connected by 10 μ_3-O^{2-} ions in the plane of the molecule and two μ-$PhCH_2CO_2^-$ groups one above and one below the plane. Thus, a useful description of **1** is as a small piece of a Mn oxide mineral held within a nonplanar ring of Mn^{III} ions. The overall core has a slightly chairlike structure, as emphasized by the side view in Figure 2. The remaining 14 μ-$PhCH_2CO_2^-$ ligands, 2 μ-MeO^- groups (bridging Mn1 and Mn7a, and their symmetry equivalents), and 6 terminal MeOH molecules provide the peripheral ligation of the complete complex.

All the Mn ions are six-coordinate with near-octahedral geometry, and their assigned oxidation states were established by charge considerations, bond valence sum calculations (Table 3), and the clear Jahn−Teller (JT) distortions of the Mn^{III} ions, which take the form of axial elongations. As expected, the JT elongated Mn^{III}−O bonds (2.106(3)−2.313(6) Å) are significantly longer than the other Mn^{III}−O bonds (1.875(3)−1.970(3) Å) and are aligned roughly parallel to each other in the direction perpendicular to the plane of the cluster (Figure 2). This is in contrast to the very similar Mn_{16} cluster previously reported by Murray and co-workers, in which only 8 of the 10 Mn^{III} ions experience JT elongation,

Table 2. Selected Bond Distances (Å) and Angles (deg) for **1**

Mn1−O1	1.901(2)	Mn6−O12a	1.909(2)
Mn1−O1a	2.313(6)	Mn6−O19	1.872(2)
Mn1−O2	2.199(3)	Mn6−O21	1.883(3)
Mn1−O3	1.941(3)	Mn6−O22	1.882(2)
Mn1−O4	2.182(12)	Mn7−O18	1.875(3)
Mn1−O21a	1.896(3)	Mn7−O21	1.915(2)
Mn1−O25a	1.931(3)	Mn7−O23	2.160(4)
Mn2−O1	1.899(3)	Mn7−O24	1.960(3)
Mn2−O5	1.901(3)	Mn7−O25	1.912(3)
Mn2−O6	2.214(3)	Mn7−O26	2.244(3)
Mn2−O7	1.953(3)	Mn8−O13	1.889(3)
Mn2−O8	1.969(3)	Mn8−O18	1.888(2)
Mn2−O9	2.154(3)	Mn8−O27	2.216(3)
Mn3−O1	1.877(3)	Mn8−O28	1.944(3)
Mn3−O5	1.871(2)	Mn8−O29	2.189(3)
Mn3−O10	1.925(2)	Mn8−O30	1.965(3)
Mn3−O11	1.910(2)	Mn1···Mn2	3.339(8)
Mn3−O12	1.917(2)	Mn1···Mn3	3.384(8)
Mn3−O22a	1.899(2)	Mn1···Mn6a	3.418(8)
Mn4−O5	1.902(2)	Mn1···Mn7a	2.947(8)
Mn4−O13	1.897(3)	Mn2···Mn3	2.810(8)
Mn4−O14	2.216(3)	Mn2···Mn4	3.313(8)
Mn4−O15	1.962(3)	Mn3···Mn4	3.428(7)
Mn4−O16	1.970(3)	Mn3···Mn5	2.848(7)
Mn4−O17	2.106(3)	Mn3···Mn6	2.899(8)
Mn5−O10	1.900(3)	Mn3···Mn6a	2.846(7)
Mn5−O11	1.880(2)	Mn4···Mn5	3.452(8)
Mn5−O13	1.896(3)	Mn4···Mn8	3.435(7)
Mn5−O18	1.869(3)	Mn5···Mn6	2.821(7)
Mn5−O19	1.882(2)	Mn5···Mn7	3.388(8)
Mn5−O20	1.926(3)	Mn5···Mn8	2.798(8)
Mn6−O11	1.919(2)	Mn6···Mn3a	2.846(7)
Mn6−O12	1.929(2)	Mn6···Mn6a	2.895(10)
Mn6···Mn7	3.419(8)	Mn7···Mn8	3.328(7)
Mn7···Mn1a	2.947(8)		

Mn1a−O21−Mn7	101.33(12)	Mn5−O18−Mn7	129.62(13)
Mn2−O1−Mn1	123.00(13)	Mn5−O18−Mn8	96.24(12)
Mn2−O5−Mn4	121.19(13)	Mn6−O21−Mn1a	129.55(13)
Mn3−O1−Mn1	127.19(13)	Mn6−O22−Mn3a	97.63(12)
Mn3−O1−Mn2	96.18(12)	Mn6−O19−Mn5	97.44(11)
Mn3−O5−Mn2	96.31(11)	Mn6−O21−Mn7	128.41(13)
Mn3−O5−Mn4	130.64(13)	Mn6a−O12−Mn3	96.12(11)
Mn3−O11−Mn6	98.44(11)	Mn6a−O12−Mn6	97.91(11)
Mn3−O12−Mn6	97.83(11)	Mn7−O25−Mn1a	100.16(13)
Mn5−O10−Mn3	96.23(12)	Mn7−O18−Mn8	124.37(14)
Mn5−O11−Mn3	97.47(11)	Mn8−O13−Mn4	130.32(14)
Mn5−O13−Mn4	131.10(13)	Mn8−O13−Mn5	95.35(11)
Mn5−O11−Mn6	95.93(11)		

(21) Wadsley, A. D. *Acta Crystallogr.* **1952**, *5*, 676.
(22) Wadsley, A. D. *Acta Crystallogr.* **1955**, *8*, 165.

Table 3. Bond Valence Sums for the Mn Atoms in Complex **1**[a]

atom	Mn^{II}	Mn^{III}	Mn^{IV}
Mn(1)	3.29	*3.01*	3.16
Mn(2)	3.21	*2.94*	3.08
Mn(3)	4.17	3.82	*4.01*
Mn(4)	3.25	*2.97*	3.12
Mn(5)	4.26	3.90	*4.09*
Mn(6)	4.18	3.83	*4.02*
Mn(7)	3.29	*3.01*	3.16
Mn(8)	3.24	*2.97*	3.12

[a] The italicized value is the one closest to the charge for which it was calculated. The oxidation state of a particular atom can be taken as the nearest whole number to the italicized value.

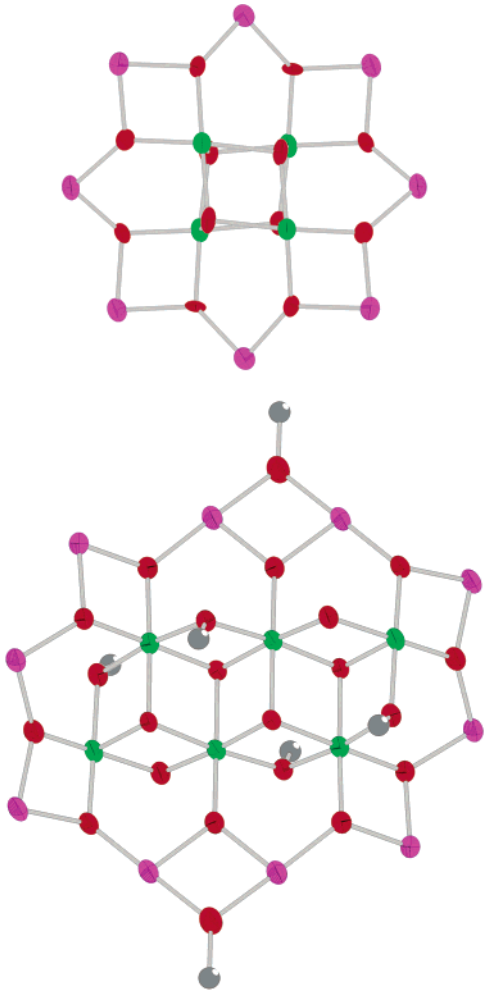

Figure 3. Comparison of the cores of Mn_{12} (top) and Mn_{16} (bottom) complexes. Color code: Mn^{IV} green; Mn^{III} purple; O red; C gray.

the remaining two experiencing JT compression with the compression axis in the plane of the cluster core.[9]

The structure of the complex has significant similarity to that of $[Mn_{12}O_{12}(O_2CR)_{16}(H_2O)_4]$: both comprise a a nonplanar Mn^{III}_x ring around a central Mn^{IV}_y unit. The cores of the Mn_{12} ($x = 8$, $y = 4$) and Mn_{16} ($x = 10$, $y = 6$) complexes are compared in Figure 3. In fact, there is a further member of this family, the Mn_{21} complex $[Mn_{21}O_{24}(OMe)_8(O_2CCH_2{}^t\text{-}Bu)_{16}(H_2O)_{10}]$ which has a Mn^{IV}_9 unit inside a nonplanar Mn^{III}_{12} ring ($x = 12$, $y = 9$).[23]

(23) Brockman, J. T.; Huffman, J. C.; Christou, G. *Angew. Chem., Int. Ed.* **2002**, *41*, 2506.

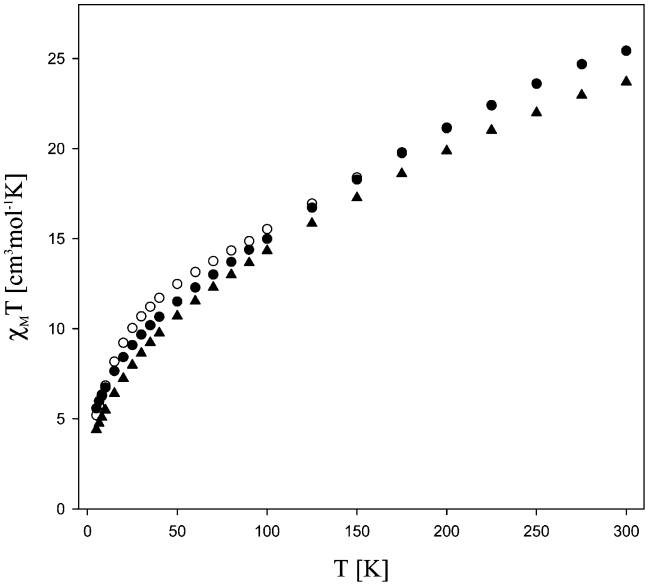

Figure 4. Plots of $\chi_M T$ vs T for complexes **1**·$4H_2O$ (○), **2** (▲), and **3**·$8H_2O$ (●).

Complexes **2** and **3** were characterized by IR spectroscopy, elemental analysis, and magnetic studies to be isostructural to **1**, and the full solution of their crystal structures was therefore not pursued.

Direct Current Magnetic Susceptibility Studies. Solid-state, variable-temperature magnetic susceptibility measurements were performed on vacuum-dried microcrystalline samples of complexes **1**·$4H_2O$, **2**, and **3**·$8H_2O$, all suspended in eicosane to prevent torquing. The dc magnetic susceptibility (χ_M) data were collected in the 5.0−300 K range in a 0.1 Tesla (T) (1000 G) magnetic field. As can be seen in Figure 4, the magnetic behavior of the three complexes is very similar. For **1**, $\chi_M T$ steadily decreases with decreasing temperature from 25.44 cm^3 mol^{-1} K at 300 K to 11.71 cm^3 mol^{-1} K at 40 K, below which the $\chi_M T$ value decreases more rapidly to 5.19 cm^3 mol^{-1} K at 5.0 K. Likewise for **2** and **3**, $\chi_M T$ gradually decreases from 23.70 cm^3 mol^{-1} K for **2** and 25.43 cm^3 mol^{-1} K for **3** at 300 K to 9.76 and 10.66 cm^3 mol^{-1} K at 40 K for **2** and **3**, respectively. Below this temperature, $\chi_M T$ again decreases more rapidly to 4.40 cm^3 mol^{-1} K for **2** and 5.58 cm^3 mol^{-1} K for **3**. For all three Mn_{16} complexes, the value of $\chi_M T$ at 300 K is much lower than that expected for a cluster of 10 Mn^{III} and 6 Mn^{IV} noninteracting ions (41.25 cm^3 mol^{-1} K for $g = 2$), suggesting that antiferromagnetic couplings dominate the overall intramolecular exchange interactions within the complexes.

With 10 Mn^{III} and 6 Mn^{IV} centers present in **1**−**3**, the total molecular spin (S) values range from 0 to 29. Owing to the size and low symmetry of the molecules, a matrix diagonalization method to evaluate the various Mn_2 pairwise exchange parameters (J_{ij}) within the Mn_{16} molecule would require diagonalizing a matrix of dimensions 4×10^{10} by 4×10^{10}, and this is clearly not readily feasible. Similarly, it is not possible to apply the equivalent operator approach based on the Kambe vector coupling method.[24] Therefore, we concentrated instead on just identifying the ground state

S value, since this would in any case dominate the low-temperature studies we performed (vide infra). In order to determine the spin ground states of complexes **1**−**3**, magnetization (*M*) data were collected in a dc magnetic field and temperature ranges of 0.1−7.0 T and 1.8−10.0 K. Attempts were made to fit the resulting data using the program MAGNET,[18] which assumes that only the ground state is populated at these temperatures, includes axial zero-field splitting (ZFS) and the Zeeman interaction with the applied field, and carries out a full powder average. However, it was not possible to obtain a good fit of the data for any of the three complexes. The problem is almost certainly that there are low-lying excited states and that these are populated even at the low temperatures employed; there is also the danger that M_S levels of excited states with *S* values greater than those of the ground state will cross in energy with the ground state in the applied dc field. In fact, low-lying excited states are expected for such a large molecule, in which the exchange interactions between the constituent atoms will lead to a high density of molecular spin states. In addition, the extensive presence of Mn_3 triangular units in the structure, as clearly evident in Figures 1 and 2, provides the textbook topology for spin frustration effects, i.e., competing antiferromagnetic exchange interactions.[25] The latter often lead to small energy differences between many of the resulting spin states. We have commented in some detail in several recent papers on the problem of low-lying excited states in such high nuclearity Mn clusters, and the resulting difficulty in reliably obtaining the ground-state *S* from magnetization measurements.[11,12,23,26] We have also described in those reports that a much more reliable method of obtaining the ground state is by the use of ac magnetic susceptibility measurements, which do not employ a dc field. For this reason, we carried out ac susceptibility studies on complexes **1**−**3**.

Alternating Current Magnetic Susceptibility Studies. In an ac susceptibility experiment, a weak field (typically 1−5 G) oscillating at a particular frequency (ν) is applied to a sample to probe the dynamics of the magnetization (magnetic moment) relaxation. Alternating current susceptibility studies were performed on vacuum-dried, polycrystalline samples of **1**−**3** in the temperature range 1.8−10 K in a zero dc field and a 3.5 G ac field oscillating at frequencies in the 5−1488 Hz range. Figure 5 shows the in-phase χ_M' component of the ac susceptibility (plotted as χ_M' vs *T*) for **1** at three frequencies (5, 10, 50 Hz); the corresponding signals for **2** and **3** are virtually identical to those for **1**. The χ_M' data can be seen to decrease steeply with decreasing temperature below 10 K. A well isolated ground state (vs *kT*) would be expected to be essentially 100% populated at these temperatures, and thus, the $\chi_M'T$ value would be expected to be essentially temperature-independent. A downward sloping $\chi_M'T$ versus *T* plot is indicative of the population of low-lying excited states with *S* values greater than the ground-state *S*, so that as they are depopulated with decreasing temperature, the $\chi_M'T$ value decreases. Extrapolation of the plot to 0 K, where only the ground state will be populated, gives a $\chi_M'T$ value of ∼3 $cm^3\ mol^{-1}$ K. This is the value expected for an $S = 2$ state with $g = 2.0$.

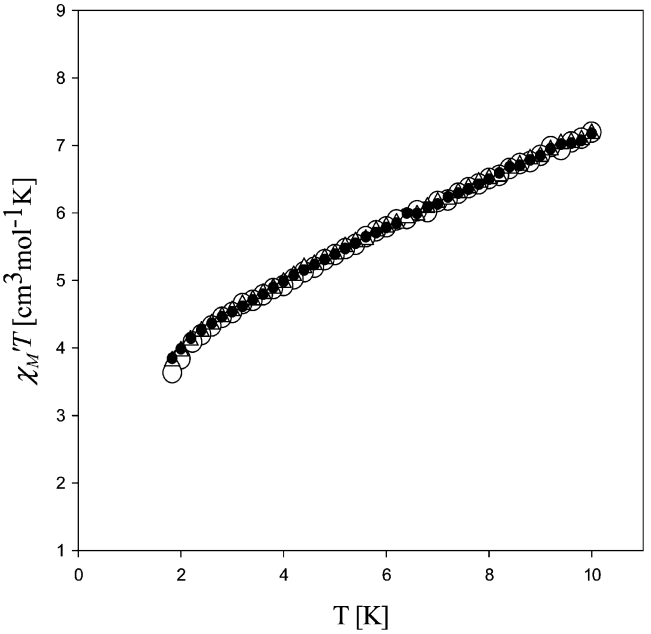

Figure 5. In-phase ac susceptibility signals (χ_M'), plotted as $\chi_M'T$, vs *T* for dried complex **1**·$4H_2O$ at 5 (●), 10 (▲), and 50 (○) Hz.

If the magnetization vector can relax fast enough to keep up with the oscillating field, then there is no out-of-phase susceptibility (χ_M'') signal, and the in-phase susceptibility (χ_M') is equal to the dc susceptibility. However, if the barrier to magnetization relaxation is significant compared to thermal energy (*kT*), then there is a nonzero χ_M'' signal and the in-phase signal decreases. In addition, the χ_M'' signal and the decrease in the $\chi_M'T$ signal will both be frequency-dependent. Such frequency-dependent ac signals are an indication of the superparamagnet-like slow relaxation of a SMM, although they do not prove an SMM because intermolecular interactions and phonon bottlenecks can also lead to such signals. The $\chi_M'T$ signals of Figure 5 show no obvious frequency-dependence except perhaps at the lowest temperatures, but the χ_M'' versus *T* plot for **1**·$4H_2O$ in Figure 6 is more sensitive and clearly shows below 3 K frequency-dependent tails of signals whose peaks lie at temperatures below the operating limit of our SQUID (1.8 K). Complexes **2** and **3** give similar results. The data thus suggest that complexes **1**−**3** may indeed exhibit the slow magnetization relaxation of a SMM.

(24) Kambe, K. *J. Phys. Soc. Jpn.* **1950**, *48*, 15.
(25) (a) Libby, E.; McCusker, J. K.; Schmitt, E. A.; Folting, K.; Hendrickson, D. N.; Christou, G. *Inorg. Chem.* **1991**, *30*, 3486. (b) McCusker, J. K.; Schmitt, E. A.; Hendrickon, D. N. High Spin Inorganic Clusters: Spin Frustration in Polynuclear Manganese and Iron Complexes. *Magnetic Molecular Materials*; Gatteschi, D., Kahn, O., Miller, J. S., Palacio, F., Eds.; NATO ASI Series 198; Kluwer: Dordrecht, 1991; pp 297−319. (c) Libby, E.; Folting, K.; Huffman, C. J.; Huffman, J. C.; Christou, G. *Inorg. Chem.* **1993**, *32*, 2549. (d) Albela, B.; El Fallah, M. S.; Ribas, J.; Folting, K.; Christou, G.; Hendrickson, D. N. *Inorg. Chem.* **2001**, *40*, 1037.
(26) (a) Brechin, E. K.; Boskovic, C.; Wernsdorfer, W.; Yoo, J.; Yamaguchi, A.; Sanudo, E. C.; Concolino, T. R.; Rheingold, A. L.; Ishimoto, H.; Hendrickson, D. N.; Christou, G. *J. Am. Chem. Soc.* **2002**, *124*, 9710. (b) Brechin, E. K.; Sañudo, E. C.; Wernsdorfer, W.; Boskovic, C.; Yoo, J.; Hendrickson, D. N.; Yamaguchi, A.; Ishimoto, H.; Concolino, T. E.; Rheingold, A. L.; Christou, G. *Inorg. Chem.*, in press.

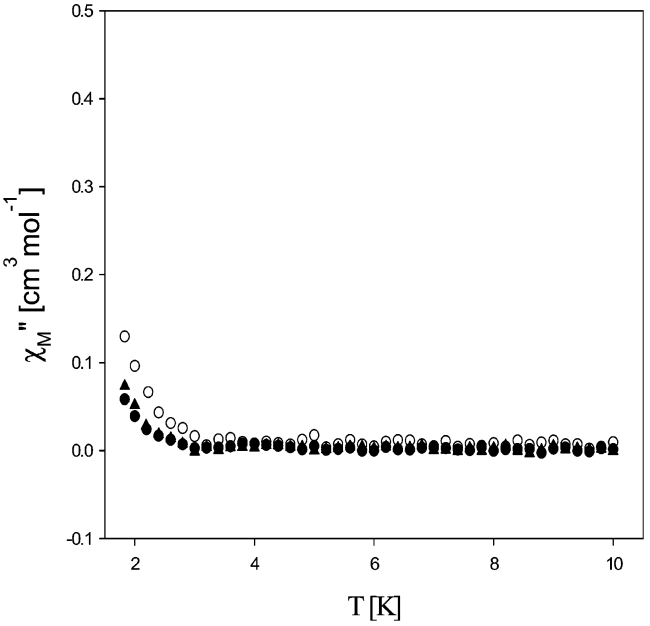

Figure 6. Out-of-phase ac susceptibility signals (χ_M'') vs T for dried complex **1**·4H_2O at 5 (●), 10 (▲), and 50 (○) Hz.

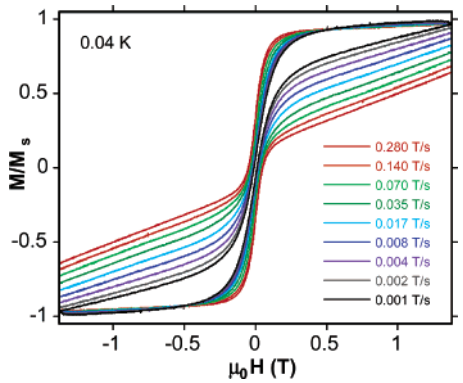

Figure 7. Magnetization (M) vs applied magnetic field hysteresis loops for complex **1**·5MeOH in the 0.001−0.280 T/s sweep rate range at 0.04 K. M is normalized to its saturation value, M_s.

It is worth noting that the behavior exhibited in Figure 6 is different from that reported for $[Mn_{16}O_{16}(OMe)_6(O_2CMe)_{16}(MeOH)_3(H_2O)_3]$·4$H_2O$[9] where a clear maximum is seen at 3.9 K at 20 Hz (4.6 K at 100 Hz) followed by the tail of a second, stronger signal whose peak lies <1.8 K. The latter signal corresponds to that for **1**−**3**.

With the ac data suggesting that **1**−**3** might be SMMs, albeit with small barriers, confirmation was sought by magnetization versus applied dc field sweeps, to see whether they display hysteresis loops, the diagnostic behavior of a magnet.

Hysteresis Studies Below 1.8 K. In order to confirm whether **1**·5MeOH is an SMM, magnetization versus applied dc field data down to 0.04 K were collected on single crystals using a micro-SQUID apparatus.[19] The resulting magnetization responses at different field sweep rates and a constant temperature of 0.04 K are shown in Figure 7. The corresponding magnetization responses at different temperatures and a fixed field sweep rate of 0.070 T/s are shown in Figure 8. In both figures are seen hysteresis loops, and their coercivities increase with increasing sweep rate and with decreasing temperature, as expected for the superparamagnet-like properties of a SMM. Hysteresis in magnetization versus field sweeps is the classical property of a magnet, and such loops are also a diagnostic feature of SMMs and superparamagnets below their blocking temperature (T_B). The data thus indicate complex **1** to be a new addition to the family of SMMs. The dominating feature in both sets of hysteresis loops is the large step (decrease in magnetization) at zero field, which we assign to ground-state QTM through the anisotropy barrier via the lowest-lying $M_S = \pm 2$ levels of the $S = 2$ manifold. The size of this step increases with decreasing sweep rate, as expected for QTM in SMMs. In other parts of the hysteresis loops, there is no clear sign of QTM steps, yet it is possible that steps are present but smeared out by broadening effects from low-lying excited states and a distribution of molecular environments (and thus a distribution of relaxation barriers) caused by disordered lattice solvent molecules and ligand disorder, both of which are present in **1**·5MeOH as described earlier. Note that the zero-field split spin manifold of low-lying excited states very likely overlaps that of the ground state, providing additional relaxation pathways that probably explain the somewhat unusual, asymmetric appearance of the hysteresis loops in Figure 8, which are taken at increasing temperatures. In addition, it is now well recognized that the magnetic properties of SMMs are sensitive to such relatively small variations in local environments and site-symmetry caused by disorder in solvent and/or ligand positions. Similar hysteresis loops with no steps characteristic of SMMs have been seen for a number of other large clusters, including Mn_{18},[26] Mn_{21},[23] Mn_{30},[12] and Mn_{84}[13] species.

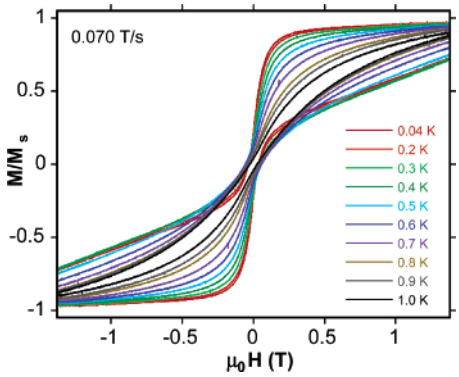

Figure 8. Magnetization (M) vs applied magnetic field hysteresis loops for **1** in the temperature range 0.04−1 K at a 0.070 T/s sweep rate. M is normalized to its saturation value, M_s.

It is worth commenting on the fact that these Mn_{16} complexes are new SMMs even though they only possess an $S = 2$ ground state. As stated earlier, the upper limit of the magnetization relaxation barrier is given by $S^2|D|$ for an integer spin system, or $4|D|$ in this case. It is clear that the D value must therefore be significantly greater than the $D = -0.5$ cm^{-1} $= -0.72$ K of $[Mn_{12}O_{12}(O_2CMe)_{16}(H_2O)_4]$; otherwise, a significant barrier would not have resulted. In fact, this is consistent with the alignment of the 10 Mn^{III} JT elongation axes very approximately all parallel, as is clear in Figure 2. A similar situation is present in the $[Mn_{12}O_{12}(O_2$-

$CMe)_{16}(H_2O)_4]$ complex,[1,2] where there are eight roughly parallel Mn^{III} JT axes. The orientation of the JT axes is crucial to the overall anisotropy (i.e., *D* value) of a molecule, because the Mn^{III} ions are the main source of magnetic anisotropy (octahedral Mn^{II} and Mn^{IV} are fairly isotropic ions) and the vectorial projection of the single-ion Mn^{III} anisotropies onto the molecular anisotropy axis (i.e. the *z* axis) determines the magnitude of the molecular *D* value. Clearly, the small value of *S* in these Mn_{16} complexes is compensated by a significant *D* value, resulting in a big enough barrier to give an SMM. Note that we do not have an estimate of *D* for these Mn_{16} molecules: we normally obtain *D* from fits of magnetization versus *H* and *T* data, or the separation of steps in the hysteresis loops, both of which are not possible for **1**−**3** for reasons already described. It will require single-crystal high-frequency EPR (HFEPR) studies to evaluate *D*, but we have not as yet been able to obtain big enough crystals for such investigations, which will in any case also be complicated by the low-lying excited states. It is also worth noting that it is a pity that the spin of **1**−**3** is indeed so low, because with 10 near-parallel JT axes, a spin more comparable to the $S = 10$ of $[Mn_{12}O_{12}(O_2CMe)_{16}(H_2O)_4]$ would almost certainly have led to a barrier larger than that of this Mn_{12} complex, which is still the "best" (i.e., highest barrier) SMM in the literature.

Conclusions. The reductive aggregation of MnO_4^- in MeOH in the presence of substituted acetic acid has proven a convenient route to three mixed-valent ($6Mn^{IV}$, $10Mn^{III}$) and trapped-valent Mn_{16} clusters. The complexes contain an interesting planar Mn^{IV}_6 unit held within a nonplanar ring of 10 Mn^{III} ions. The complex has only an $S = 2$ ground state, but the near-parallel alignment of the Mn^{III} JT elongation axes provides sufficient molecular anisotropy to result in a small barrier to magnetization relaxation and hysteresis loops at very low temperatures. Hence, complexes **1**−**3** are new members of the growing family of single molecule magnets (SMMs). Further novel species have been isolated from the use of the reductive aggregation procedure, and these will be reported soon.

Acknowledgment. We thank the National Science Foundation for support of this work.

Supporting Information Available: X-ray crystallographic data in CIF format for complex **1**·5MeOH. This material is available free of charge via the Internet at http://pubs.acs.org.

IC048906J